2023 IEEE International Conference on Robotics and Automation (ICRA 2023)
May 29 - June 2, 2023. London, UK

Gait Event Detection with Proprioceptive Force Sensing in a Powered Knee-Ankle Prosthesis: Validation over Walking Speeds and Slopes

Emily G. Keller, Curt A. Laubscher, and Robert D. Gregg

Abstract— **Many powered prosthetic devices use load cells to detect ground interaction forces and gait events. These sensors introduce additional weight and cost in the device. Recent proprioceptive actuators enable an algebraic relationship between actuator torques and ground contact forces. This paper presents a proprioceptive force sensing paradigm which estimates ground reaction forces as a solution to detect gait events without a load cell. A floating body dynamic model is obtained with constraints at the center of pressure representing foot-ground interaction. Constraint forces are derived to estimate ground reaction forces and subsequently timing of gait events. A treadmill experiment is conducted with a powered knee-ankle prosthesis used by an able-bodied subject walking at various speeds and slopes. Results show accurate gait event timing, with pooled data showing heel strike detection lagging by only 6.7 $\pm$ 7.2 ms and toe off detection leading by 30.4 $\pm$ 11.0 ms compared to values obtained from the load cell. These results establish proof of concept for predicting gait events without a load cell in powered prostheses with proprioceptive actuators.**

I. Introduction

Individuals with lower-limb loss are hindered in their mobility with a reduction in physical activity. Passive prosthetic legs are not able to provide the net positive work required for many daily tasks such as sit-stand transitions, or stair ascent and descent [1]–[3]. Emerging powered prostheses have the potential to address this limitation through the use of joint actuators and sensors, but with the trade-off of significantly increasing device weight and cost.

Limb/prosthesis weight plays a significant role in the biomechanics of walking [4], [5]. To provide comfortable mobility resembling healthy able-bodied locomotion, it is essential to reduce the weight of powered prostheses as much as possible. Load cells are typically included in powered prosthetic legs to detect gait events for the purpose of control [6]. These sensors contribute to the weight of the prosthesis, and their cost can be significant. For example, the M3564F 6-axis load cell (Sunrise Instruments, Nanning, China) used in our powered knee-ankle prosthesis [7] costs $3,300 MSRP and weighs 200 g. The Open Source Leg [8] also has a commercial 6-axis load cell. The Vanderbilt leg [9] uses a custom uniaxial load cell in the shank, and the Utah leg [10], [11] incorporates a custom multi-axial load cell in the pyramid adapter. These sensors add a considerable amount of cost, weight, and/or complexity to these devices. Additionally, these sensors add a point of failure to the devices, as do all sensors. Ideally, we would want to not only remove the load cell or force sensor, but avoid adding any other kind of sensor for the purpose of gait event detection.

Load cells or force sensors have previously been avoided in various contexts. Inertial measurement units, accelerometers, and gyroscopes have been used for gait event detections but lack the ability to provide ground reaction force data [12], [13]. Alternatively, utilizing mechanical transparency in the actuator so that motor current is directly proportional to output actuation torque has been shown in the literature. Luca and Mattone identified robot collisions using only joint encoder data [14]. Bhatia similarly investigated contact localization where non-collocated sensors were used to measure the state of their robot and detect contact anywhere on their robotic device [15]. Wensing et al. directly controlled ground contact force through the actuator torques of a quadrupedal robot [16]. These mechanically transparent actuators require low reflected inertia and minimal frictional losses, which are key properties of direct drive and quasi-direct drive actuators (i.e., a high-torque motor with a low-ratio transmission) [7], [17], [18]. These so-called *proprioceptive actuators* can exploit an algebraic relationship between actuator torque and ground contact force, thus making exteroceptive sensors unnecessary [16]. This type of actuator has been utilized in the literature for the application of proprioceptive force control to achieve quadrupedal bounding [16] and bipedal pronking motions [19]. Recently, quasi-direct drive actuators have been implemented in powered prosthetic legs [7], [20], but the concept of force proprioception has not yet been explored in this context.

In order to remove load cells from powered prosthetic legs, this paper proposes a proprioceptive force *sensing* method for solving the inverse problem of proprioceptive force control: estimating the ground reaction force (GRF) from known actuator torques. Similar to proprioceptive force control, proprioceptive sensing is enabled by proprioceptive actuators, and renders a load cell redundant. The primary contribution of this paper is accurate detection of foot contact events using this novel proprioceptive sensing method in a powered knee-ankle prosthesis. The contents of this paper are as follows: Section II describes the hardware and outlines the system parameters. Section III covers the main theory of proprioceptive sensing for GRF estimation and gait event detection. Section IV details the experimental methods for an able-bodied human subject experiment with the powered prosthesis from [7]. Sections V and VI present and discuss

This work was supported by the National Institute of Child Health & Human Development of the NIH under Award Number R01HD094772. This work was also supported by the National Science Foundation under Award Number 1949869. The content is solely the responsibility of the authors and does not necessarily represent the official views of the NIH or NSF.

Emily G. Keller, Curt A. Laubscher, and Robert D. Gregg are with the Department of Robotics, University of Michigan, Ann Arbor, MI 48109. Contact: {egkeller, claub, rdgregg}@umich.edu

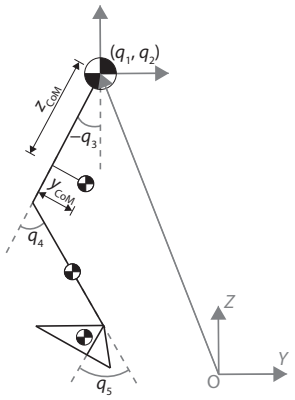

Fig. 1. The prosthetic side is modeled as a three-link system with a configuration vector defined by the Cartesian coordinates of the hip and the joint angles.

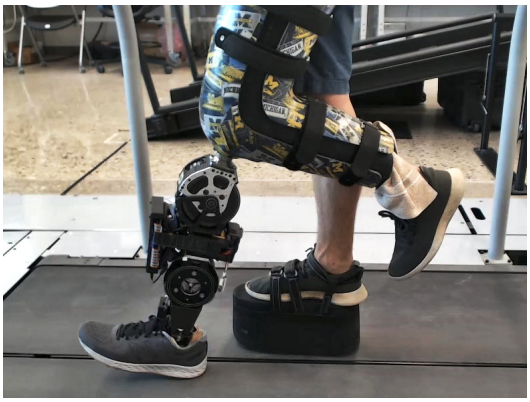

Fig. 2. Experimental setup showing an able-bodied subject using the powered knee-ankle prosthesis with a leg-bypass adapter.

the results which show the proprioceptive force sensing method reasonably estimates ground reaction forces and provides accurate gait event timings.

II. Device and Modeling

A. Hardware Description

The powered knee-ankle prosthesis used in this paper is described in detail in [7]. Both joints use an ILM 85×26 motor kit (RoboDrive, Seefeld, Germany). These motors have a manufacturer-rated continuous torque of 2.6 Nm and a peak torque of 8.3 Nm, each paired with a single-stage stepped-planet compound planetary gear transmission giving a 22:1 speed-reduction ratio. This quasi-direct drive actuator design has low reflected inertia and friction, and thus can be used as a proprioceptive actuator. The motor's input current is proportional to the actuator's output torque [7], allowing the applied torque to be accurately estimated without directly measuring the torque at the output with a torque sensor. The overall weight of the device is 6.09 kg, 0.20 kg of which is from the M3564F 6-axis load cell not including its mounting components. Note this sensor remained on the prosthesis for the purpose of comparison and validation in this study.

B. Model Parameters

The system is modeled using a floating, planar, serial-link system with three links corresponding to the thigh, shank, and foot. A diagram of the model can be seen in Fig. 1.

For this paper, the model assumes the prosthetic leg is used by an able-bodied subject wearing a leg-bypass interface adapter (Fig. 2). The center of mass (CoM) for the thigh link includes the user's biological shank constrained at a right angle behind the prosthesis. The intact leg segment lengths and relative CoM positions used for each segment are from body segment proportions reported in Winter [21]. This put the CoM at $y_{\mathrm{CoM}} = 0.0547H$ posterior to the hip and $z_{\mathrm{CoM}} = 0.1587H$ distal to the hip where H is the subject's height without the device on. The CoM of the prosthetic shank is approximated at the midpoint of that segment. The foot CoM is approximated halfway between the ankle and the ground and halfway through the total length of the foot, which is approximately 27% of the total foot length in front of the ankle joint. The mass of the rest of the body is modeled as a point mass at the hip. The subject's total mass includes the mass of the device. For simplicity, the foot is assumed to be a rigid body even though the carbon fiber foot on the device allows for some flexion. The length used for the thigh link in the model is the measured distance between the subject's greater trochanter and the knee joint of the device while the subject is in the bypass adapter. The shank length, ankle height, and foot length are measured from the device. The masses of the shank and foot were measured as built. The shank and foot moments of inertia were determined from the SolidWorks® CAD model. A summary of the model parameters, derived from the prosthesis, are shown in Table I.

TABLE I

Model Parameters of the Subject-Prosthesis System

Parameter	Value
Subject Height	1.727 m
System Mass	80.100 kg
Thigh Length	0.578 m
Shank Length	0.351 m
Ankle Height from Ground	0.095 m
Total Foot Length	0.300 m
Shank Mass	5.609 kg
Foot Mass (with Shell & Shoe)	1.140 kg
Shank Inertia	0.043 kg·m^2
Foot Inertia	0.001 kg·m^2
Reflected Inertia	0.056 kg·m^2

III. Theory

A. Phase-Based Center of Pressure

The gait cycle defines locomotion and starts and ends with the heel strike of one leg. Phase is a measure of progression through the gait cycle that monotonically increases from 0 to 1. In this work, phase was determined based on the thigh angle measured by a prosthesis-mounted inertial measurement unit as described in [22]. To estimate the GRF acting on the system, the effective point of contact with the ground is needed. The center of pressure (CoP) was used as this point, defined to be negative in the anterior direction and positive in the posterior direction. During stance, an empirical model was used to determine the CoP as a function of phase. Using offline data from an able-bodied subject using a bypass interface, the CoP c and phase s_{st} during stance were fit with a spline. This was accomplished using

data across the nine tasks described in Section IV-B to ensure the phase-based CoP was task-independent. From the offline data, the CoP was calculated at each time index i as follows:

$$c(i) = \begin{cases} \dfrac{F_{\mathrm{x}}(i) \cdot z_{\mathrm{a}} - M_{\mathrm{y}}(i)}{F_{\mathrm{z}}(i)}, & F_{\mathrm{z}}(i) > \beta \\ c(i-1), & F_{\mathrm{z}}(i) \leq \beta \end{cases} \tag{1}$$

where F_{x} is the horizontal force from the load cell, z_{a} is the vertical distance from the ankle to the ground, M_{y} is the moment about the ankle from the load cell, F_{z} is the vertical force from the load cell, and β is a tunable threshold chosen as 300 N. During swing, the CoP was set to be 10 cm behind the ankle along the bottom of the foot. This value was chosen heuristically for accurate gait event detection. There is also a saturation limit of -17 cm corresponding to the end of the device's shoe. Prior offline analysis indicated that this limit allows for accurate detection of TO across all nine tasks. The combination of the swing value, saturation, and spline fit form a phase-based piecewise function for CoP.

B. Proprioceptive Force Sensing

The dynamics of the three-link system are modeled using the Euler-Lagrange method. Constraints are applied such that the CoP is pinned to the ground. The dynamics and constraint equations of motion are

$$D(q)\ddot{q} + C(q,\dot{q})\dot{q} + G(q) = J(q,c)^T\lambda + Su \tag{2}$$

$$\dot{J}(q,c)\dot{q} + J(q,c)\ddot{q} = 0 \tag{3}$$

where $q \in \mathbb{R}^5$ is the configuration vector, $D(q) \in \mathbb{R}^{5\times5}$ is the inertia matrix, $C(q,\dot{q}) \in \mathbb{R}^{5\times5}$ is the Coriolis and centrifugal matrix, $G(q) \in \mathbb{R}^5$ is the gravity vector, $J(q,c) \in \mathbb{R}^{2\times5}$ is the contact Jacobian depending on CoP c, $\lambda \in \mathbb{R}^2$ is the contact force vector ensuring the constraint equation is satisfied, $S \in \mathbb{R}^{5\times2}$ is the input mapping selector matrix, and $u \in \mathbb{R}^2$ is the input torque vector at the controllable joints. The torque at the hip was not included in u since it is not accessible from the controller. Offline numerical analysis suggests that including hip torque does not significantly impact the magnitude of the GRF calculation. The dynamics and constraint equations can be rewritten as

$$\begin{bmatrix} D & -J^T \\ J & 0 \end{bmatrix}\begin{bmatrix} \ddot{q} \\ \lambda \end{bmatrix} + \begin{bmatrix} C\dot{q} + G - Su \\ \dot{J}\dot{q} \end{bmatrix} = \begin{bmatrix} 0 \\ 0 \end{bmatrix} \tag{4}$$

which can then be solved for λ:

$$\begin{bmatrix} \ddot{q} \\ \lambda \end{bmatrix} = \underbrace{-\begin{bmatrix} D & -J^T \\ J & 0 \end{bmatrix}^{-1}}_{Z}\begin{bmatrix} C\dot{q} + G - Su \\ \dot{J}\dot{q} \end{bmatrix} \tag{5}$$

The inverse of the first matrix is:

$$Z = -\begin{bmatrix} D^{-1} - D^{-1}J^T\Lambda JD^{-1} & D^{-1}J^T\Lambda \\ -\Lambda JD^{-1} & -\Lambda \end{bmatrix} \tag{6}$$

where $\Lambda = (JD^{-1}J^T)^{-1}$ is the operational-space inertia matrix. Therefore the equation to solve for the GRF λ is

$$\lambda = \Lambda JD^{-1}(C\dot{q} + G - Su) + \Lambda\dot{J}\dot{q}. \tag{7}$$

Assuming reasonably slow speeds, the equation simplifies to

$$\lambda = \Lambda JD^{-1}(G - Su). \tag{8}$$

This 2-element vector of horizontal and vertical GRFs is a function of the configuration q, CoP c, and control inputs u. These calculated forces are defined with respect to the world coordinate system, whereas the load cell's forces are with respect to the foot's coordinate system. Therefore, a rotation matrix based on the task's incline angle was multiplied to the left of λ for comparison with load cell forces.

C. Proprioceptive Gait Event Detection

The vertical GRF was used to detect gait events. Heel strike (HS) was detected when the GRF exceeded a tunable threshold, and toe off (TO) was detected when GRF dropped below a separate tunable threshold. Foot contact is defined as the period after HS detection and before TO detection.

IV. Experimental Methods

A. Hybrid Impedance-Kinematic Controller

The device used the phase-based controller described in detail in [22]. This controller employs a continuously-varying impedance paradigm during stance and position control during swing. The vector of knee and ankle joint torques during stance is given by

$$\tau_{\mathrm{st}} = m(K(\hat{s}_{\mathrm{st}},\chi)(\theta_{\mathrm{eq}}(\hat{s}_{\mathrm{st}},\chi) - \theta) - B(\hat{s}_{\mathrm{st}},\chi)\dot{\theta}). \tag{9}$$

In this equation $\hat{s}_{\mathrm{st}}$ is the stance phase estimate and χ is the task defined as the combination of walking speed and incline. The joint stiffness K, damping B, and equilibrium angle θ_{eq} are modeled as functions of phase and task to best predict able-bodied joint torques given able-bodied joint kinematics [22]. For this paper, the correct task was given to the controller, not estimated in real-time as in [22]. The amount of torque was scaled by the mass of the user m, since the impedance parameters are normalized by mass.

During swing, the control strategy in [22] employs a proportional-derivative controller to track desired joint kinematics, θ_{d} and $\dot{\theta}_{\mathrm{d}}$, which are modeled as functions of phase and task based on able-bodied walking data [1]. Swing torque is then calculated as

$$\tau_{\mathrm{sw}} = k_{\mathrm{p}}(\theta_{\mathrm{d}}(\hat{s}_{\mathrm{sw}},\chi) - \theta) + k_{\mathrm{d}}(\dot{\theta}_{\mathrm{d}}(\hat{s}_{\mathrm{sw}},\chi) - \dot{\theta}), \tag{10}$$

where $\hat{s}_{\mathrm{sw}}$ is the swing phase estimate. The gain k_{p} for the knee and ankle are 1 and 3.5 Nm/deg, respectively, and the gain k_{d} for the knee and ankle are 0.08 and 0.05 Nm·s/deg, respectively, as defined in [22].

The controller determines stance vs. swing based on thresholds of load cell measurements in [22], but our proprioceptive method uses GRF estimates as described in Section III-C. A minimum dwell time of 100 ms ensures unexpected rapid switching does not occur. To ensure a smooth transition from stance to swing, a time-varying weight ω_{sw} was used. At TO, ω_{sw} increases at a constant rate from 0 to 1 over 0.25 s for the knee and 0.05 s for the ankle. Ankle smoothing

is faster to avoid toe-stubbing. The torque applied by the controller is given by

$$\tau = \begin{cases} \tau_{\mathrm{st}}, & \text{during Stance} \\ \omega_{\mathrm{sw}}\tau_{\mathrm{sw}}, & \text{during Swing} \end{cases} \tag{11}$$

At HS, the similarity in the equilibrium angles made smoothing unnecessary.

B. Experimental Protocol

An able-bodied subject (26 years, 74.0 kg, 173 cm) with experience using the powered prosthesis was recruited for participation. The experimental protocol was approved by the Institutional Review Board of the University of Michigan (HUM00166976). The subject wore a bypass adapter for compatibility with the prosthesis (Fig. 2). Measurements of the subject-prosthesis system were used for deriving the parameters in the dynamic model described in Section II-B, which are summarized in Table I.

The experimental protocol entailed an acclimation session and a main evaluation session on the same day. In both parts, the subject walked on a split-belt treadmill (Bertec, Columbus, Ohio, USA), shown in Fig. 2. For the acclimation session, the subject walked at 0.8 m/s with no incline. The controller detected gait events from GRF measured by the load cell. In addition to providing the subject time to become acclimated to the hardware, this portion of the experiment was used to tune proprioceptive GRF thresholds for gait event detection that were used in the subsequent experiments (reported later). Offline analysis of previously recorded data showed that thresholds tuned based only on this one task were adequate for gait event detection in all other tasks.

For the main evaluation session, the controller used gait events detected from the proprioceptive force sensing method. Nine tasks were performed: three level walking conditions at 0.8, 1.0 and 1.2 m/s, three incline walking conditions at 3, 5 and 7 deg, and three decline walking conditions at 3, 5 and 7 deg. All incline and decline conditions had a treadmill speed of 1.0 m/s. The duration of each task was 1.5 minutes, and the subject was allowed to rest for any amount of time between tasks. For analysis, only the middle 50 strides were used to ensure steady-state walking. The load cell data were recorded from these tasks and used as a point of comparison for GRF estimation and timing of gait events.

V. Results

All recorded data had a sampling frequency of 250 Hz. The data recorded from the acclimation session were used to determine the tunable parameters. The GRF thresholds for HS and TO detection were selected as 200 and 50 N, respectively. These values proved to be sufficient for detecting gait events for all tasks in the subsequent evaluation portion of the experiment and are expected to be valid for all future subjects. The subject commented that they could not feel a difference between the two gait event detection methods (based on load cell GRF data vs. proprioceptive GRF estimates). Two outlier strides where the subject stumbled slightly during the 7 deg decline task were manually removed from the following analysis, but 50 strides were still analyzed for this condition. No outliers were observed for any other task.

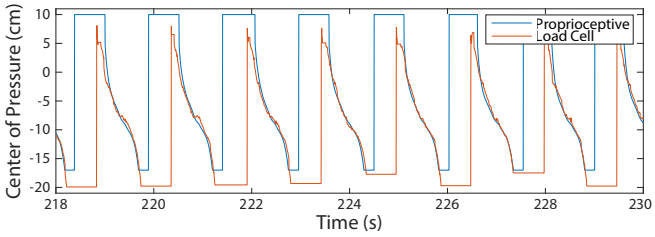

Fig. 3. Estimated and actual center of pressure over time for proprioceptive force sensing methods vs. load cell force sensing method. Positive values correspond to posterior position along the foot and negative values correspond to anterior position along the foot.

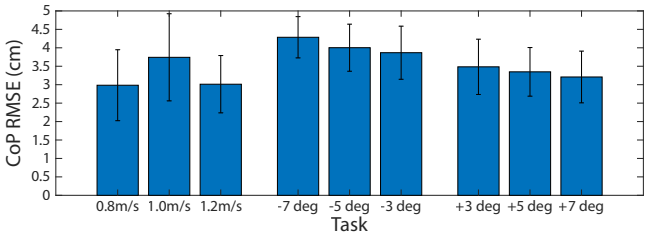

Fig. 4. Center of pressure (CoP) root-mean-square error (RMSE) with ± 1 standard deviation over nine task conditions. Negative ramp angles correspond to declines, and positive ramp angles correspond to inclines.

A. Phase-Based Center of Pressure

The phase-based estimation of CoP for a representative task (1.0 m/s with no incline) from the evaluation session is shown in Fig. 3. For comparison, the CoP calculated from load cell data using (1) is also shown. Other tasks exhibited similar CoP matching.

Portions of the data where the actual CoP is a constant value and the estimated CoP is 10 cm translates roughly to the swing phase of gait. The mean and standard deviation (STD) of the root-mean-square-error (RMSE) are reported in Fig. 4. Due to the different swing-phase CoP definitions, reported values only consider the error during stance as determined by the proprioceptive sensing method.

B. Ground Reaction Force Estimation

The GRF estimate using the proprioceptive sensing method for the same representative task is shown in Fig. 5 with GRF thresholds for HS and TO superimposed. For a point of comparison, GRF values measured by the load cell are also included. The average GRF of that task is also shown, partitioned by gait events detected by the load cell.

C. Event Detection

Figure 6 shows the mean timing error with standard deviations for HS and TO timing when compared to the load cell timings. A positive error indicates that the proprioceptive sensing method had a late detection with respect to the load cell, while a negative error indicates early detection. The error $\pm$ STD for all 50 strides pooled over all tasks (450 strides total) was 6.7 $\pm$ 7.2 ms (0.43 $\pm$ 0.46 %) for HS timing and –30.4 $\pm$ 11.0 ms (1.95 $\pm$ 0.70 %) for TO timing.

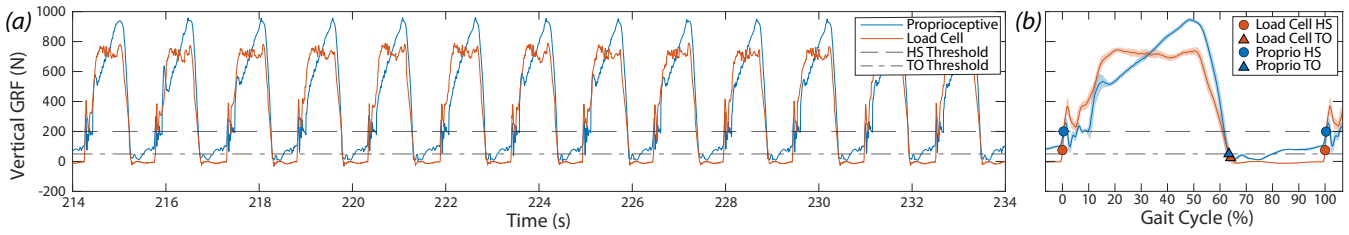

Fig. 5. *(a)* Vertical ground reaction force estimated by the proprioceptive sensing method from the level-ground 1.0 m/s trial, compared to load cell measurements. Thresholds for heel strike (HS) and and toe off (TO) are shown. *(b)* Average step with ± 1 standard deviation and gait event detections.

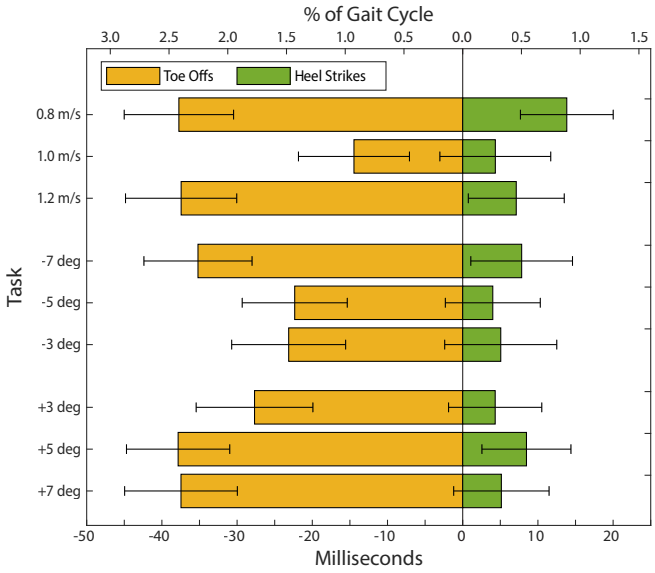

Fig. 6. Task-specific heel strike and toe off timing errors relative to load cell detection (zero), expressed in time (bottom axis) and % gait cycle (top axis). Negative values indicate early detection relative to load cell.

D. Joint Kinematics and Kinetics

To examine the effect of proprioceptive gait event detection on the prosthetic joint patterns, we compared the acclimation session using the load cell to the matching proprioception evaluation trial (level-ground 0.8 m/s) in Fig. 7. Both sets of data were partitioned into strides using the corresponding HS detection method. The average of the strides was taken and plotted over gait cycle percentage. The able-bodied trajectory from [1] was added for reference.

VI. Discussion

A. Phase-Based Center of Pressure

For the majority of stance, the phase-based CoP function is a good estimate for the actual CoP determined by the load cell (Fig. 3). A large contributor to the error seen in Fig. 4 comes from the function saturating at the lower limit of -17 cm around late stance until TO is detected. Another major contributor to the error is from the CoP staying at its initial value (10 cm) in early stance while the phase variable saturated at 0 (a feature that ensures phase remains within the bounds from 0 to 1).

Various observations can be made from Fig. 4. There appears to be a trend between the ground angle and CoP RMSE. As the angle of the ground increases from -7 deg (decline) to $+7$ deg (incline), the RMSE decreases. The difference in the mean RMSEs of the ± 7 deg tasks is 1.1 cm, which is greater than STD of either case. This suggests there is a relationship between the ground angle and CoP estimation accuracy. This reduction in error is attributed to a better estimation of CoP near HS and TO for the incline task than the decline task. At HS, phase begins to increase earlier in the incline task than the decline task, thus phase is saturated less during stance. At TO, the CoP gets closer to the extreme edge of the foot in incline, as opposed to decline which requires less push-off, thus the CoP saturation matches the actual value better. Level walking at the same speed of 1.0 m/s fits the trend. The RMSE for 0.8 and 1.2 m/s tasks are lower than that of the 1.0 m/s task, though the cause for this difference is unclear. Ultimately, the observed CoP error did not undermine the proprioceptive force sensing method.

B. Ground Reaction Force Estimation

The double-lobed shape for vertical GRF that is typically observed in able-bodied walking is not seen whether GRF is measured with the load cell or estimated by the proprioceptive sensing method (Fig. 5). This can be explained by how locomotion and weight support during bypass prosthetic walking is quite different than normative able-bodied walking. The estimated GRF can be seen skewing to the right, underestimating in early stance and overestimating in late stance. This was a consistent trend across all tasks. The contribution to GRF from gravity in (8) was the major contributor for the early-stance, and the contribution to GRF from commanded torque was the major contributor for mid- to late-stance. The magnitude of the contribution due to gravity overall is lower than that of the command torque, resulting in the observed skewing. There are a few possible explanations for this behavior. Previous offline analyses suggest the system is reliant on having an accurate dynamic model, which could affect the quality of the results. Relatedly, the structure of the dynamic model would likely influence estimation behavior. For instance, the flexible foot was assumed rigid, and there is not a rigid connection between the prosthesis bypass interface and the user's thigh.

Another observation from the proprioceptive GRF in Fig. 5 is an occasional reduction at around 25% of stance phase, which is more frequent and pronounced in ramp walking. This can also be attributed to the contribution to GRF from the commanded torques and gravity both having low magnitudes around this period. Moreover, the proprioceptive sensing method assumes the system is pinned at the CoP in the constraint equation (3). However, this assumption is

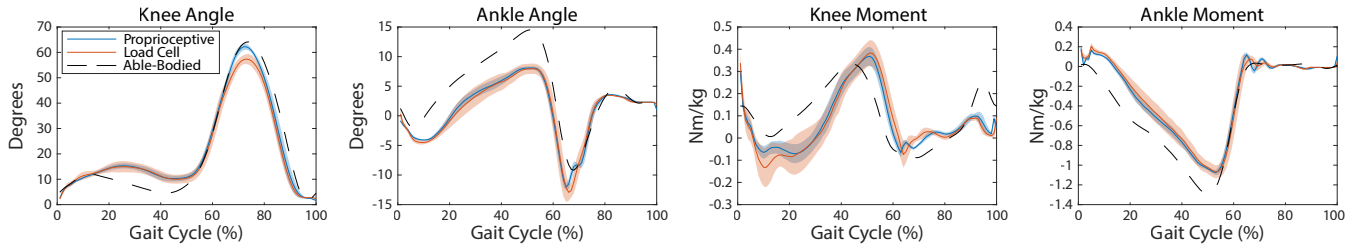

Fig. 7. Averaged joint kinematics and kinetics with ± 1 standard deviation shaded regions using proprioceptive force sensing vs. load cell force sensing. Able-bodied reference data is shown.

inaccurate during swing phase, and therefore the method calculates small forces during swing as seen in Fig. 5.

C. Event Detection

The HS and TO timing errors were within milliseconds of the load cell timings, with HS detection generally being late and TO detection being early. The STD bars in Fig. 6 suggest that, for some tasks, HS detection may also occur early. Late HS detection is due to compounding factors. The false GRF estimation during swing, discussed in the previous section, requires that the threshold for HS detection be set sufficiently high to avoid false detections. This ultimately led to HS detection often being delayed in comparison to the load cell. Early TO detection occurred due to the steeper slope in the GRF estimation from the proprioceptive sensing method in comparison to the GRF measured by the load cell during push-off in late-stance. The two outlier strides which were removed from the 7 deg decline task were caused by the GRF being sufficiently low during stance such that a false TO event was detected. This could potentially be mitigated by increasing the minimum dwell time.

All tasks exhibited similar HS timing errors. The only exception was with the 0.8 m/s with no incline task, though the cause is unclear. Level walking at 1.0 m/s showed lower timing errors than the other two level walking conditions, though the cause is unclear. The variation in the mean TO timing errors across the ramp walking tasks could be attributed to random variation.

D. Joint Kinematics and Kinetics

The joint kinematics and kinetics for the load cell method and the matching task for the proprioceptive sensing method both roughly resemble that of able-bodied data (Fig. 7). In addition, the two trials were quite similar, with the largest differences in the kinematics occurred in early swing. Peak knee flexion was about 5 deg higher in the proprioceptive method in comparison to the load cell method, and peak ankle plantar-flexion was about 0.9 deg higher in the load cell method. The knee and ankle joint moments remained within expected variation throughout the majority of the gait cycle and did not exhibit any significant differences. Considering the similarity in the joint kinematics and kinetics, any differences in the gait event timings had little to no impact on the performance of the controller.

E. Limitations and Future Work

One limitation of the phase-based CoP estimate, common among all model-based paradigms, is that if the input to the function strays from the expected values, the output may be inaccurate. For example, if phase does not reflect actual progression of gait, the computed value for CoP will be inaccurate. This will consequently affect the calculation of GRF and subsequent detection of HS and TO events, possibly leading to unsafe conditions. This was not observed in practice. Future work for this includes changing the estimation method for CoP to be the zero-moment point [23], which would not require an empirical model and would be based on the calculated forces as opposed to phase. Alternatively, a disturbance observer for force estimation would also not require task or activity-specific models for CoP [24].

A limitation of the proposed proprioceptive sensing method is its reliance on an accurate dynamic model derived from the weight and height of the subject. Future work entails improving accuracy in the model and considering adaptive approaches to avoid the need for an accurate model prior to the experiment. This has the potential to improve GRF estimation, which would be necessary for considering other control strategies reliant on accurate knowledge of GRF for things such as impedance modulation [25], [26].

Finally, our validation of the proprioceptive sensing method was limited to a single able-bodied subject using the powered prosthesis. This paper serves as a proof of concept to motivate future endeavors involving trials with more subjects, particularly individuals with lower-limb loss, and more tasks such as ascending and descending stairs [27].

VII. Conclusion

This paper presented a proprioceptive force sensing paradigm to estimate ground reaction forces and subsequently gait events. We developed a phase-based function that is able to accurately estimate center of pressure throughout stance. An able-bodied experiment was conducted to evaluate the proposed proprioceptive sensing method on a powered knee-ankle prosthesis during level and ramp walking. The experiment showed that the method reasonably estimates ground reaction forces and provides accurate gait event timings. These results suggest that proprioceptive force sensing is a promising alternative to load cells for the purpose of estimating gait events. This could reduce cost and weight in powered prostheses and locomotive devices with proprioceptive actuators. Our hope is that cheaper and lighter prosthetic devices will enable more people to be able to use powered devices in their daily lives to easily perform any task they desire.

REFERENCES

[1] E. Reznick, K. R. Embry, R. Neuman, E. Bolívar-Nieto, N. P. Fey, and R. D. Gregg, "Lower-limb kinematics and kinetics during continuously varying human locomotion," *Scientific Data*, vol. 8, no. 1, p. 282, Dec. 2021.

[2] R. Riener, M. Rabuffetti, and C. Frigo, "Stair ascent and descent at different inclinations," *Gait & Posture*, vol. 15, no. 1, pp. 32–44, Feb. 2002.

[3] J. Camargo, A. Ramanathan, W. Flanagan, and A. Young, "A comprehensive, open-source dataset of lower limb biomechanics in multiple conditions of stairs, ramps, and level-ground ambulation and transitions," *J. Biomechanics*, vol. 119, p. 110320, Apr. 2021.

[4] R. W. Selles, J. B. Bussmann, R. C. Wagenaar, and H. J. Stam, "Effects of prosthetic mass and mass distribution on kinematics and energetics of prosthetic gait: A systematic review," *Archives of Physical Medicine and Rehabilitation*, vol. 80, no. 12, pp. 1593–1599, Dec. 1999.

[5] R. C. Browning, J. R. Modica, R. Kram, and A. Goswami, "The Effects of Adding Mass to the Legs on the Energetics and Biomechanics of Walking," *Medicine & Science in Sports & Exercise*, vol. 39, no. 3, pp. 515–525, Mar. 2007.

[6] R. R. Torrealba and E. D. Fonseca-Rojas, "Toward the Development of Knee Prostheses: Review of Current Active Devices," *Applied Mechanics Reviews*, vol. 71, no. 3, p. 030801, May 2019.

[7] T. Elery, S. Rezazadeh, C. Nesler, and R. D. Gregg, "Design and Validation of a Powered Knee–Ankle Prosthesis With High-Torque, Low-Impedance Actuators," *IEEE Trans. Robotics*, vol. 36, no. 6, pp. 1649–1668, Dec. 2020.

[8] A. F. Azocar, L. M. Mooney, J.-F. Duval, A. M. Simon, L. J. Hargrove, and E. J. Rouse, "Design and clinical implementation of an open-source bionic leg," *Nature Biomedical Engineering*, vol. 4, no. 10, pp. 941–953, Oct. 2020.

[9] B. E. Lawson, J. Mitchell, D. Truex, A. Shultz, E. Ledoux, and M. Goldfarb, "A Robotic Leg Prosthesis: Design, Control, and Implementation," *IEEE Robotics & Automation Magazine*, vol. 21, no. 4, pp. 70–81, Dec. 2014.

[10] T. Lenzi, M. Cempini, L. Hargrove, and T. Kuiken, "Design, development, and testing of a lightweight hybrid robotic knee prosthesis," *Int. J. Robotics Research*, vol. 37, no. 8, pp. 953–976, Jul. 2018.

[11] L. Gabert and T. Lenzi, "Instrumented pyramid adapter for amputee gait analysis and powered prosthesis control," *IEEE Sensors Journal*, vol. 19, no. 18, pp. 8272–8282, 2019.

[12] J. Taborri, E. Palermo, S. Rossi, and P. Cappa, "Gait partitioning methods: A systematic review," *Sensors*, vol. 16, no. 1, p. 66, 2016.

[13] H. F. Maqbool, M. A. B. Husman, M. I. Awad, A. Abouhossein, N. Iqbal, and A. A. Dehghani-Sanij, "A real-time gait event detection for lower limb prosthesis control and evaluation," *IEEE Transactions on Neural Systems and Rehabilitation Engineering*, vol. 25, no. 9, pp. 1500–1509, 2017.

[14] A. de Luca and R. Mattone, "Sensorless Robot Collision Detection and Hybrid Force/Motion Control," in *IEEE Int. Conf. Robotics & Automation*, Barcelona, Spain, 2005, pp. 999–1004.

[15] A. Bhatia, "Direct-drive Hands: Making Robot Hands Transparent and Reactive to Contacts," Ph.D. dissertation, Carnegie Mellon University, Jun. 2022.

[16] P. M. Wensing, A. Wang, S. Seok, D. Otten, J. Lang, and S. Kim, "Proprioceptive Actuator Design in the MIT Cheetah: Impact Mitigation and High-Bandwidth Physical Interaction for Dynamic Legged Robots," *IEEE Trans. Robotics*, vol. 33, no. 3, pp. 509–522, Jun. 2017.

[17] S. Seok, A. Wang, M. Y. Chuah, D. J. Hyun, J. Lee, D. M. Otten, J. H. Lang, and S. Kim, "Design principles for energy-efficient legged locomotion and implementation on the mit cheetah robot," *IEEE/ASME Trans. Mechatronics*, vol. 20, no. 3, pp. 1117–1129, 2014.

[18] G. Kenneally, A. De, and D. E. Koditschek, "Design principles for a family of direct-drive legged robots," *IEEE Robotics and Automation Letters*, vol. 1, no. 2, pp. 900–907, 2016.

[19] J. Yu, J. Hooks, X. Zhang, M. Sung Ahn, and D. Hong, "A Proprioceptive, Force-Controlled, Non-Anthropomorphic Biped for Dynamic Locomotion," in *IEEE Int. Conf. Humanoid Robots*, Beijing, China, 2018.

[20] J. Zhu, C. Jiao, I. Dominguez, S. Yu, and H. Su, "Design and backdrivability modeling of a portable high torque robotic knee prosthesis with intrinsic compliance for agile activities," *IEEE/ASME Trans. Mechatronics*, 2022.

[21] D. A. Winter, *Biomechanics and motor control of human movement*, 4th ed. Hoboken, N.J: Wiley, 2009.

[22] T. Best, C. Welker, E. Rouse, and R. Gregg, "Data-driven variable impedance control of a powered knee-ankle prosthesis for adaptive speed and incline walking," *IEEE Trans. Robotics*, 2022.

[23] M. Vukobratović and B. Borovac, "Zero-Moment Point - Thirty Five Years of its Life," *Int. J. Humanoid Robotics*, vol. 1, no. 1, pp. 157–173, Mar. 2004.

[24] G. Bledt, P. M. Wensing, S. Ingersoll, and S. Kim, "Contact model fusion for event-based locomotion in unstructured terrains," in *2018 IEEE International Conference on Robotics and Automation (ICRA)*. IEEE, 2018, pp. 4399–4406.

[25] H. Warner, P. Khalaf, H. Richter, D. Simon, E. Hardin, and A. J. van den Bogert, "Early evaluation of a powered transfemoral prosthesis with force-modulated impedance control and energy regeneration," *Medical Engineering Physics*, vol. 100, p. 103744, 2022.

[26] A. M. Simon, N. P. Fey, K. A. Ingraham, S. B. Finucane, E. G. Halsne, and L. J. Hargrove, "Improved weight-bearing symmetry for transfemoral amputees during standing up and sitting down with a powered knee-ankle prosthesis," *Archives of Physical Medicine and Rehabilitation*, vol. 97, no. 7, pp. 1100–1106, 2016.

[27] R. J. Cortino, E. Bolivar-Nieto, T. K. Best, and R. D. Gregg, "Stair ascent phase-variable control of a powered knee-ankle prosthesis," in *Int. Conf. Robotics and Automation*, Philadelphia, PA, USA, May 2022, p. 5673–5678.